


J.M. REY  
D. MARINOV  
D.E. VOGLER  
M.W. SIGRIST 

# Investigation and optimisation of a multipass resonant photoacoustic cell at high absorption levels

ETH Zurich, Institute of Quantum Electronics, Laser Spectroscopy and Sensing Laboratory, Hoenggerberg, 8093 Zurich, Switzerland

Received: 28 October 2004

Published online: 8 December 2004 • © Springer-Verlag 2004

**ABSTRACT** A theoretical and experimental investigation of photoacoustic (PA) signals in a resonant multipass PA cell with high background absorption (up to  $29\text{ m}^{-1}$ ) is presented. An analogous electric transmission line model including discontinuity inductances at cross section changes was used to model the first longitudinal acoustic mode of the multipass PA cell equipped with two buffer volumes. This model was validated with experimentally obtained results and used to predict the behaviour of the PA cell for different multipass arrangements and different buffer volume diameters. The highest PA signal is obtained for high pass number and large buffer radius. Increasing the absorption coefficient of the medium enhances the PA signal until a maximum is reached, leading to a minimum for the PA signal sensitivity. For a given background absorption, the number of passes required to maximise the sensitivity depends on the absorption coefficient. The model allows the determination of the best-suited number of passes for a given absorption coefficient and cell geometry.

PACS 82.80.Kd; 42.62.Fi; 82.80.Gk

## 1 Introduction

Photoacoustic (PA) spectroscopy is a powerful technique for detecting traces of gases due to its intrinsically high sensitivity, large dynamic range, and comparatively simple experimental set-up [1–3]. The detection limit of this technique is mainly determined by the light source used and the PA cell design. The sensitivity of PA cells has been improved by acoustic amplification of the PA signal thanks to the use of resonant PA cells [4–11]. Resonant cells have also been designed for multipass or intracavity operation [12–16]. Cell windows generate synchronous noise which has been minimized by introducing acoustic baffles [17], by the development of a “windowless” [18] or differential cell [19, 20].


Owing to its high sensitivity, PA spectroscopy is usually applied to the detection of weak absorption signals. In the case of low optical absorption, a uniform heat deposition along the light beam is observed and the generated PA signal depends only on the quantity of absorbed power. Nevertheless, even

if the low absorption case is frequent, strong background absorption is sometimes present. This is particularly the case for in-situ monitoring where carbon dioxide, ammonia, alcohol or water absorptions can interfere with the species under investigation. At high absorption, the incident light power decreases exponentially in the PA cell and the course of the absorption along the beam path has to be taken into account for modelling the PA signal. Due to the longer absorption path in multipass cells, the exponential radiation decay affects the PA response more strongly than the one of single-pass cells. High-absorption phenomena have been observed previously in pulsed PA spectroscopy [21, 22]. These effects are important since they influence both the PA response in presence of a highly absorbing background and the dynamic range of a PA system.

In order to obtain a better understanding of high absorption effects in resonant multipass PA cells, this paper presents an experimental investigation of PA signals generated in a strongly absorbing gas medium. A theoretical model based on electric transmission line circuit elements is used to describe the acoustic properties of the multipass PA cell employed. The validity of this model is tested by comparing the obtained simulated results with experimental ones. Finally, the validated model is used to derive guidelines concerning the design and optimisation of resonant multipass PA cells.

## 2 Experimental arrangement

A cw sealed-off line-tunable  $^{12}\text{CO}_2$  laser (Edinburgh Instruments, model PL-2-L) with an active power stabilisation based on a piezo-driven output-coupling mirror is used as light source. A diffraction grating mounted in a Littrow arrangement and controlled by a stepper motor allows to set the desired laser transition. A cw output power of up to 3 W is available depending on the chosen  $\text{CO}_2$  laser transition. The  $\text{CO}_2$ -laser radiation is amplitude-modulated by passing through a chopper (New Focus, model 3501). The back reflection of the chopper is used to monitor the laser transition with a spectrum analyser (Optical Engineering, model 16-A) and the actual laser power by a power-meter (Coherent Inc., Model 205). The transmitted excitation light is coupled into the home-built multipass PA cell. The PA cell consists of a Herriott multipass arrangement [23] around a resonant PA cell. With a mirror spacing of 700 mm, our Herriott cell ex-

 Fax: +41-1-633-1230, E-mail: sigrist@iqe.phys.ethz.ch

hibits 18 passes and this number can even be extended to 80 by a mirror adjustment. As a result more laser power is available inside this multipass resonant cell for the generation of the PA signal than in a usual one-pass arrangement. The geometry of the resonant PA cell is depicted in Fig. 1. The cell is placed inside the multipass arrangement and consists of five cylinders: the actual resonator (length 120 mm, radius 25 mm), two adjacent buffer volumes with larger diameters (length 60 mm, radius 60 mm) and two cylinders (radius 20 mm) connecting the buffer volumes to the ZnSe-Brewster windows. The cell dimensions, particularly its diameter, are adapted to the number of passes and the beam diameter of the CO<sub>2</sub> laser. The inner cylindrical part enables the excitation of a pronounced longitudinal acoustic resonance whereas the buffer volumes reduce acoustic noise caused by the gas flow and by heating of the Brewster windows. A radial microphone array with 16 electret microphones (Sennheiser KE 4-211-2) is placed in a plane perpendicular to the optical axis at the centre of the resonator where the first longitudinal resonance of the pressure amplitude reaches its maximum. More detailed information about the resonant multipass PA cell can be found elsewhere [16].

The signal taken from the microphone array is monitored by a lock-in amplifier (Stanford Research Systems SR830). Since a resonant PA cell is used, the chopper frequency has to be carefully locked to the actual resonance frequency of the cell which fluctuates mainly due to variations of the temperature and the gas composition particularly in field measurements. This is achieved by periodical scans of the modulation frequency across a small range around the resonance frequency and consecutively choosing a modulation frequency that corresponds to the peak of the frequency scan. The data for the laser power, modulation frequency, PA signal amplitude and phase are recorded on a computer through a GPIB interface. Additional data for temperature and pressure measured in the PA cell are also collected. The whole setup is installed in a trailer for field studies. Successful measurement campaigns have been reported earlier [24].

In order to investigate the effect of high-background absorption, gaseous samples with high absorption were prepared by using dynamic headspace extraction [25]. This technique vaporizes a part of a volatile sample by continuously bubbling a gas through its liquid phase. Methanol vapour has been used as absorption medium because of its high vapour pressure (50.2 mbar at 277 K [26]) and high absorption cross-

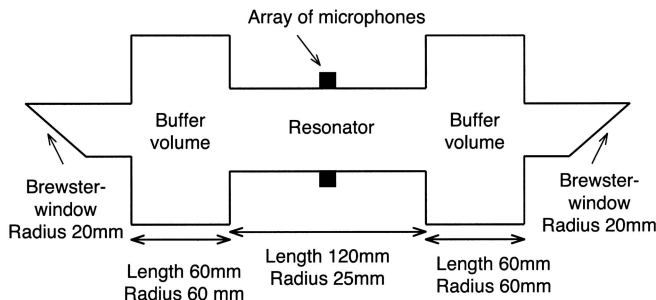


**FIGURE 1** Schematic representation of the PA cell used in this work. The cell consists of five coaxial cylinders connected in series, the microphone array is at the centre of the resonator

section at the 9P34 CO<sub>2</sub> laser line (absorption coefficient: 17 m<sup>-1</sup> at 1 mol %, 950 mbar and 293 K [27]). Pure liquid methanol (Merck, pro analysis) was used in the bubbling flask and its temperature stabilized at  $T = 277$  K with a thermostatic bath (Huber, TC50). The liquid methanol temperature was thus always below room temperature ( $T = 293$  K) to avoid any methanol condensation in the connecting tubes or the PA cell. Pure nitrogen (Pangas, 4N5) was employed as bubbling/carrier gas and a fritted head used to reduce bubble size and improve methanol evaporation. The resulting methanol-containing nitrogen flow was then diluted with pure nitrogen in order to control the final methanol concentration of the gas flowing through the PA cell. This procedure presents two main advantages: the methanol content of the generated sample can be varied in real-time and the use of a continuous sample flow reduces adsorption and desorption problems.

### 3 Transmission line model

In PA spectroscopy an acoustic wave is generated by the absorption of the amplitude-modulated light. Under the assumption that the acoustic wavelength exceeds the overall dimensions of the resonator, the PA cell and its acoustic properties can be modelled by discrete acoustic impedances. Using the formal equivalence with electric transmission line theory, the acoustical pressure amplitude  $p$  and volume velocity  $v$  are replaced by the voltage amplitude  $U$  and the electric current  $I$  in the corresponding electric line circuit [10, 28, 29]. If the acoustic wavelength is equal or smaller than the spatial dimensions of the resonator, longitudinal standing waves occur in the cavity and modelling by discrete acoustic impedances fails. In such a case, the resonator should be treated with the extended Helmholtz resonator (EHR) theory [30]. This approach derives the correct analogous acoustic impedances by dividing the resonator into subcells of infinitesimal length. The connection of the infinitesimal subcells in series yields the characteristic acoustic impedance  $Z_{\omega}^c$  (1) and the propagation constant  $\gamma_{\omega}^c$  (2) of an electric transmission line describing the propagation of a longitudinal sound wave along the tube. Retransformation of the electric transmission line into a simple T-circuit [31] consisting of discrete acoustic elements ((3) and (4)) yields the analogue electric circuit which represents the acoustic cell.

$$Z_{\omega}^c = \frac{\rho c}{\pi r_i^2} \sqrt{\frac{1 + d_v/r_i}{1 + (\gamma - 1)d_t/r_i}} \times \left[ 1 - \frac{i}{2} \left( \frac{(\gamma - 1)}{r_i/d_v + 1} - \frac{(\gamma - 1)}{r_i/d_t + (\gamma - 1)} \right) \right] \quad (1)$$

$$\gamma_{\omega}^c = \frac{i\omega}{c} \sqrt{\left(1 + \frac{d_v}{r_i}\right) \left(1 + (\gamma - 1)\frac{d_t}{r_i}\right)} \times \left[ 1 - \frac{i}{2} \left( \frac{(\gamma - 1)}{r_i/d_t + (\gamma - 1)} + \frac{1}{r_i/d_v} \right) \right] \quad (2)$$

$$Z_{ai} = Z_{\omega}^c \tanh\left(\frac{\gamma_{\omega}^c L_i}{2}\right) \quad (3)$$

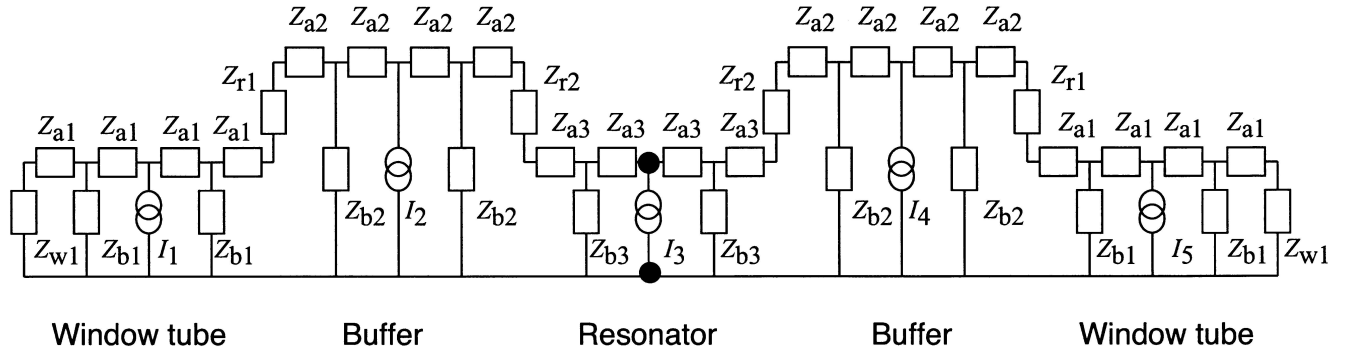


**FIGURE 2** Analog electric transmission line circuit used to model the first longitudinal acoustic mode of the five-cylinder PA cell.  $Z_{ij}$  ( $i = a, b, r, w$  and  $j = 1, 2, 3$ ) represent the impedances and  $I_i$  ( $i = 1$  to  $5$ ) the current sources (see text). The voltage  $U$  is calculated across the  $I_3$  current source

$$Z_{bi} = \frac{Z_{\omega}^c}{\sinh(\gamma_{\omega}^c L_i)} \quad (4)$$

Here  $\omega = 2\pi\nu$  is the circular modulation frequency of the light excitation,  $\rho$  the gas density,  $c$  the speed of sound and  $\gamma = C_p/C_v$  the ratio of specific heats at constant pressure and volume. The impedances  $Z$  correspond to the different branches (denoted by a and b) of the T-circuits (see Fig. 2) and the index  $i$  ( $i = 1$  to  $5$ ) refers to the different tubes with length  $L_i$  and radius  $r_i$ . The thickness  $d_v$  and  $d_t$  of the viscous and thermal boundary layers are given by :

$$d_v = \sqrt{\frac{2\mu}{\rho\omega}} \quad \text{and} \quad d_t = \sqrt{\frac{2K}{\rho\omega C_p}} \quad (5)$$

where  $\mu$  and  $K$  stand for the viscosity and heat conductivity, respectively. The PA cell employed in this work consists of five cylinders connected in series. The microphones used to detect the PA signal are located in the middle of the central tube. Using the electric transmission line analogy, each cylinder is represented by two T-circuits connected to a current source. Each T-circuit corresponds to one half of the cylinder while the current source represents the acoustic wave excitation generated by light absorption within the tube. In each tube the acoustic excitation is represented by a current source ( $I_i$ ,  $i = 1$  to  $5$ ) with an amplitude proportional to the absorbed light power and to the spatial overlap between the propagating light beam and the pressure distribution of the acoustic mode under investigation. These current sources have the same frequency and phase as the excitation light. When two tubes of different circular section are joined together, an additional impedance ( $Z_{ri}$ ) has to be introduced. In the case of an ideal viscousless fluid and for acoustic wavelengths much longer than the tube radii, this impedance can be approximated by [32]:

$$Z_{ri} = i\omega \sqrt{\frac{8\rho}{3\pi^2 r_{\min}}} H\left(\frac{r_{\min}}{r_{\max}}\right) \quad (6)$$

where  $r_{\min}$  and  $r_{\max}$  correspond to the radius of the smaller tube and larger tube, respectively, and  $H(r_{\min}/r_{\max})$  represents a discontinuity correction factor derived in [32]. The cell windows are represented by the impedances  $Z_{w1}$  which are usually infinite. Figure 2 presents the electric network used

to model the five-cylinders PA cell. To simulate the PA signal due to longitudinal acoustic waves, the first step consists in calculating the impedances  $Z_{ai}$ ,  $Z_{bi}$  and  $Z_{ri}$  ((3), (4) and (6)) and current sources ( $I_i$ ) at the modulation frequency of the excitation light. Then the electric network is solved to obtain the voltage  $U$  across the current source  $I_3$  which is proportional to the microphone signal. This procedure can be repeated for different excitation frequencies to obtain the frequency response of the PA cell and its resonance frequency.

#### 4 Results and discussion

The frequency response of the PA cell has been investigated using a total flow of 332 ml/min. This flow consisted of 300 ml/min of pure nitrogen mixed with 32 ml/min of nitrogen saturated with methanol at  $T = 277$  K. The gas temperature in the cell was 295.7 K and the pressure 955 mbar, which yields an absorption coefficient of  $8.6 \text{ m}^{-1}$  at the 9P34  $\text{CO}_2$  laser line [27]. Figure 3 shows the measured frequency response of the cell around 1270 Hz with estimated experimental errors. The solid line presents the frequency response calculated with the transmission line model described

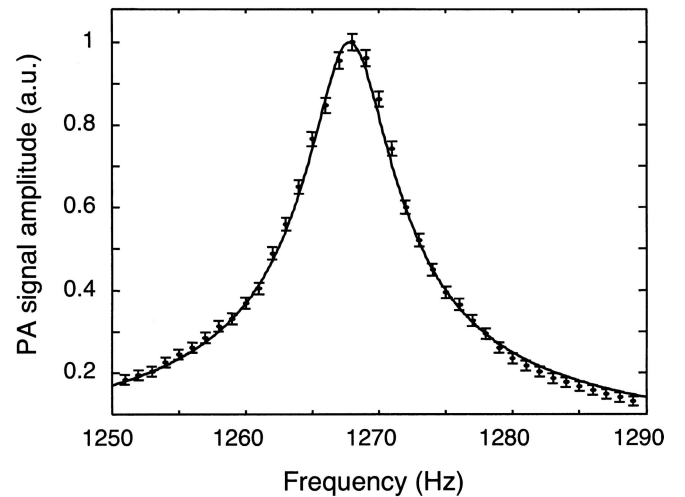


**FIGURE 3** PA cell frequency response of the first longitudinal mode. The dots represent the experimental PA signal amplitude with the estimated error bars and the solid line represents the result of the simulation (absorption coefficient:  $8.6 \text{ m}^{-1}$ , resonator length: 120 mm, buffer radius: 60 mm, resonator radius: 25 mm, number of passes: 18)

Specific heat capacity	$C_p$	1005	(J kg <sup>-1</sup> K <sup>-1</sup> )	[33]
$C_p/C_v$	$\gamma$	1.4		[33]
Density	$\rho$	1.16	(kg m <sup>-3</sup> )	[33]
Thermal conductivity	$K$	$2.598 \times 10^{-2}$	(W m <sup>-1</sup> K <sup>-1</sup> )	[34]
Viscosity	$\mu$	$1.79 \times 10^{-5}$	(kg m <sup>-1</sup> s <sup>-1</sup> )	[34]
Speed of sound	$c$	350.85	(m s <sup>-1</sup> )	[This work]
		351	(m s <sup>-1</sup> )	[35]
Acoustic impedance at window	$Z_w$	$4 \times 10^6$	(kg m <sup>-4</sup> s <sup>-1</sup> )	[This work]

**TABLE 1** Thermodynamic data used in the acoustic transmission line model. Except for those determined in this work, the data refer to pure nitrogen

above. The data for the thermodynamic parameters used in the model were not fitted to the experimental results but taken for pure nitrogen from literature (see Table 1). The actual cell dimensions are also directly introduced in the model. The only two fitting parameters are the speed of sound and the acoustic impedance ( $Z_{w1}$ ) at the cell windows. The obtained acoustic impedance at the window amounts to  $4 \times 10^6 \text{ kg m}^{-4} \text{ s}^{-1}$  and is thus truly large, as expected from theory. The speed of sound used for the fit is 350.85 m/s and thus in agreement with the 351.0 m/s found in reference [35] for nitrogen at 295.7 K and 1013 mbar. The resonant mode presented in Fig. 3, with a maximum at 1268 Hz and FWHM of 10.7 Hz, can be assigned to the first longitudinal mode of the central inner tube of the cell and its frequency almost corresponds to the one calculated using the end correction for open resonators [3, 36]. The PA amplitude was measured at this resonance frequency of the cell for different gas absorption coefficients. The absorption coefficient was varied by changing the pure nitrogen flow from 40 to 500 ml/min and the methanol-saturated (at  $T = 277 \text{ K}$ ) nitrogen flow between 2 and 30 ml/min. The gas temperature in the PA cell was 293 K and its pressure 950 mbar. The PA signal amplitude for absorption coefficients between  $0.4 \text{ m}^{-1}$  and  $29 \text{ m}^{-1}$  is presented in Fig. 4. The error bars show the estimated experimental errors and the solid line presents the amplitude calculated using the transmission line model with the same parameters as used for Fig. 3. At low absorption coefficient ( $< 1 \text{ m}^{-1}$ ), the PA sig-

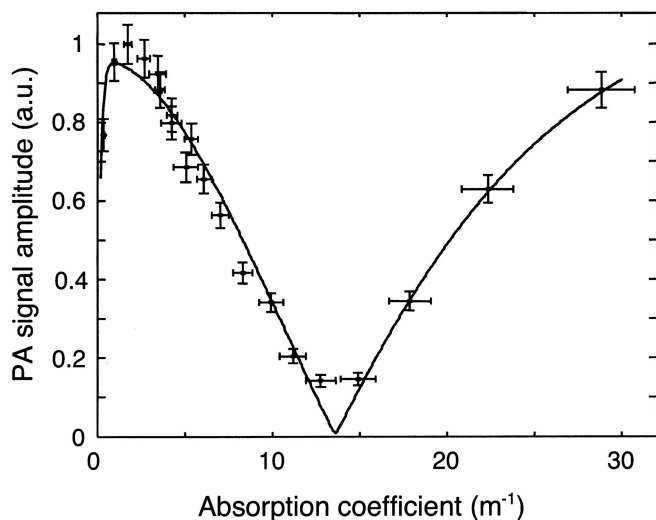


**FIGURE 4** PA signal amplitude vs. absorption coefficient. The dots represent the experimental results with the estimated error bars and the solid line shows the result of the simulation (buffer radius: 60 mm, resonator radius: 25 mm, number of passes: 18)

nal amplitude increases with the absorption coefficient. When the absorption coefficient is further increased, the PA signal decreases, reaches a minimum and finally increases again. This behaviour yields a maximum and a minimum of the PA signal amplitude and shows that a given PA signal could correspond to three different absorption coefficients (Fig. 4). Figures 3 and 4 demonstrate the excellent agreement between the modelled and experimental PA cell behaviour. This implies that a transmission line model which includes a simple discontinuity inductance at cross section changes is suitable to accurately describe the first longitudinal mode of a cylindrical PA cell without introducing any resonator end correction. The most widely used end correction [36] is based on the limiting case where the buffer radius is much larger than the resonator radius whereas the model presented here involves both buffer and resonator radii and can thus be applied for small cross section changes as in other previous models [10, 28].

The good agreement between experimental and calculated data indicates that the model can be used to predict the behaviour of the PA signal for different multipass arrangements or different buffer volume diameters. The effect of these two parameters on the absolute value of the PA signal and on the sensitivity (derivative of PA signal with respect to the absorption coefficient [37]) has been investigated for absorption coefficients up to  $5 \text{ m}^{-1}$ . Since the absorption coefficient of a compound is proportional to its concentration, an increase of the PA signal sensitivity improves the minimal detectable concentration change. Increasing the PA signal sensitivity is especially important for the detection of small absorptions caused by the species of interest in the presence of a highly absorbing background. In this case, the PA cell design has to be adapted to provide the highest sensitivity at the given background absorption.

Figure 5a and b present the calculated PA signal amplitude and absolute sensitivity for three different buffer volume radii (40 mm, 50 mm and 60 mm) while keeping the other parameters (number of passes: 18) constant and identical to those used for the model validation. These figures show that the amplitude of the PA signal increases with the buffer radius and that the highest absolute sensitivity is obtained for the largest radius (60 mm) except for the  $0.97\text{--}1.07 \text{ m}^{-1}$  absorption coefficient range. At low absorption levels (below  $0.05 \text{ m}^{-1}$ ) and without kinetic cooling effect [24, 38–40], the PA signal is proportional to the absorption of the compound present in the cell [1]. At higher absorption levels, the PA signal is no longer proportional to the absorption coefficient but shows a maximum (Fig. 5a). This results in a drastic change of the PA signal sensitivity with respect to the absorption coefficient as depicted in Fig. 5b. For the 18-pass cell, a rather large resonator radius ( $r = 25 \text{ mm}$ ) is required to accommodate the

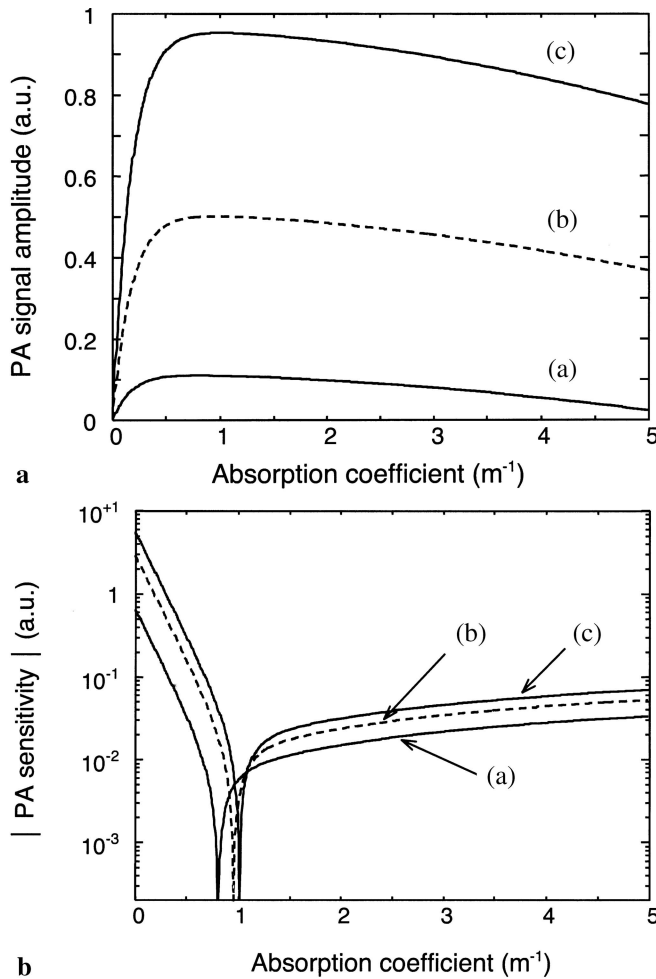


**FIGURE 5** (a) Calculated PA signal amplitude vs. absorption coefficient for different buffer radii: (a) buffer radius: 40 mm, (b) buffer radius: 50 mm and (c) buffer radius: 60 mm (resonator radius: 25 mm, number of passes: 18) (b) Absolute value of the calculated PA signal sensitivity (derivative of PA signal with respect to the absorption coefficient) vs. absorption coefficient for different buffer radii: (a) buffer radius: 40 mm, (b) buffer radius: 50 mm and (c) buffer radius: 60 mm (resonator radius: 25 mm, number of passes: 18)

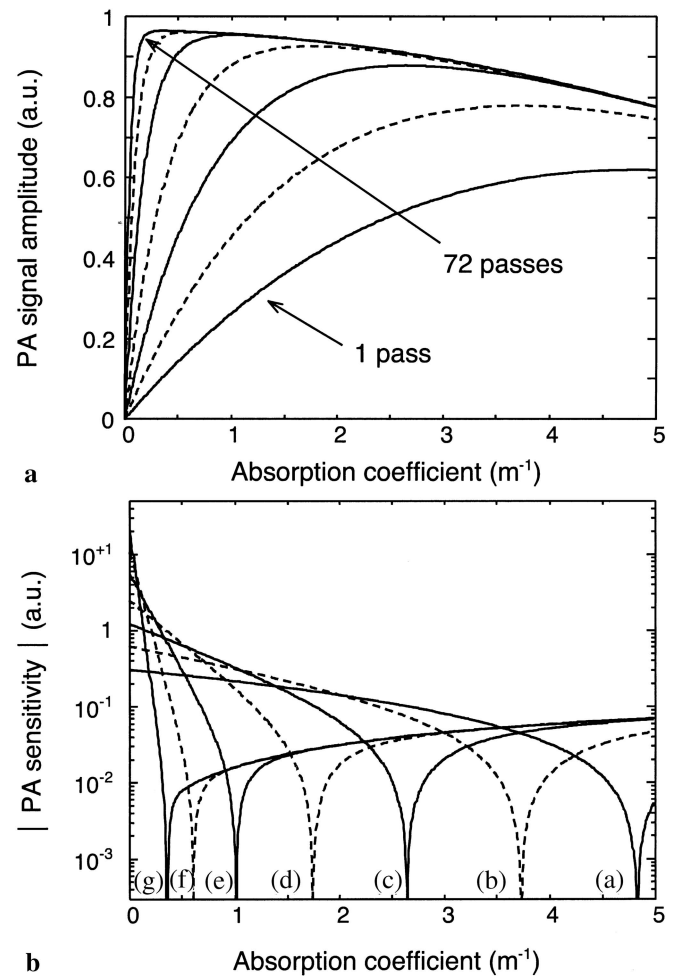


**FIGURE 6** (a) Calculated PA signal amplitude vs. absorption coefficient for 1, 2, 4, 8, 18, 36 and 72 number of passes (buffer radius: 60 mm, resonator radius: 25 mm) (b) Absolute value of the calculated PA signal sensitivity (derivative of PA signal with respect to the absorption coefficient) vs. absorption coefficient for 1 (a), 2 (b), 4 (c), 8 (d), 18 (e), 36 (f) and 72 (g) number of passes (buffer radius: 60 mm, resonator radius: 25 mm)

Herriot's arrangement and the buffer radii have to be larger than the resonator radius. The increase of the PA signal with the buffer radius originates from the better confinement of the acoustic wave within a resonator with a large buffer radius. This confinement reduces losses at the buffer/resonator junction. Each of the three radii (40 mm, 50 mm and 60 mm) shows a PA signal maximum and a corresponding PA signal sensitivity minimum. Since these minima occur at slightly different absorption coefficients, the buffer volume radius has to be carefully chosen if a background absorption close to  $1 m^{-1}$  is expected. For absorption coefficients below  $0.97 m^{-1}$  and above  $1.07 m^{-1}$ , a radius of 60 mm is preferable since it yields both the highest signal amplitude and sensitivity.

The calculated PA signal and the sensitivity for different number of passes (1, 2, 4, 8, 18, 36 and 72) using a 60 mm buffer radius are presented in Fig. 6a and b. Changing the number of passes from 1 to 72 affects the PA signal and sensitivity more strongly than changing the buffer radii. An increase of the absorption coefficient yields a steeper PA signal rise for a high pass number until a maximum is reached.

Figure 6a shows that the PA signal maximum simultaneously gets higher and moves to lower absorption coefficient when the number of passes increases. The PA signal sensitivity is proportional to the number of passes for absorption coefficients smaller than  $0.001 m^{-1}$ . This is due to the negligible reduction of the light intensity even after the 72 passes at low absorption. Increasing the absorption coefficient removes this linear proportionality and the number of passes required to obtain the maximum sensitivity depends on the absorption coefficient (Fig. 6b). The minimum of PA signal sensitivity takes place at a lower absorption coefficient for a high pass number. With the cell described above, this minimum moves from  $4.83 m^{-1}$  to  $0.36 m^{-1}$  by changing the pass number from 1 to 72. This has a substantial impact on the PA cell design since it provides a way to tune the position of the minimum of the PA signal sensitivity by changing the number of passes. Figure 6b allows one to determine the best suited number of passes for a given absorption coefficient. For example, the eight-pass arrangement (Fig. 6b, curve (d)) exhibits a higher sensitivity than all the other considered pass numbers for an absorp-

tion coefficient of  $0.5 \text{ m}^{-1}$ . With this absorption coefficient, the sensitivity of the eight-pass cell is two order of magnitude higher than the one observed in the 72-pass cell (Fig. 6b, curve (g)) and 2.5 time higher than the one for a single-pass cell (Fig. 6b, curve (a)).

## 5 Conclusion

The analogous electric transmission line model including discontinuity inductances at cross section changes allows the calculation of the amplitude, frequency dependence and sensitivity of the PA signal for the first longitudinal mode. On the basis of the excellent agreement between the measured and calculated data, the model is used to predict the behaviour of the PA signal for different multipass arrangements and different buffer volume diameters. The highest PA signal is obtained for high pass number and large buffer radius. Increasing the absorption coefficient of the medium enlarges the PA signal until a maximum is reached. This PA signal maximum corresponds to a minimum for the PA signal sensitivity. Increasing the buffer radius or increasing the number of passes moves the sensitivity minimum to lower absorption. However, a change of the number of passes affects the position of the sensitivity minimum more strongly and is experimentally simpler to realise than changing the buffer radius. For a given background absorption, the number of passes required to maximise the sensitivity depends on the absorption coefficient. The best-suited pass number for a given absorption coefficient and cell geometry can be obtained by simulating the PA cell response with the model presented in this work.

**ACKNOWLEDGEMENTS** The financial support by the Swiss National Science Foundation, ETH Zürich and the Alliance of Global Sustainability (AGS) is greatly acknowledged.

## REFERENCES

- M.W. Sigrist: Air Monitoring by Laser Photoacoustic Spectroscopy. In: *Air Monitoring by Spectroscopic Techniques* (Chemical Analysis Series 127), ed. by M.W. Sigrist (Wiley, New York 1994) Chapt. 4
- F.J. M. Harren, G. Cotti, J. Oomens, S. te L. Hekkert: Photoacoustic Spectroscopy in Trace Gas Monitoring. In: *Encyclopedia of Analytical Chemistry* 3, ed. by R.A. Meyers (Wiley, Chichester 2000) pp. 2203–2226
- A. Miklòs, P. Hess: *Rev. Sci. Instrum.* **72**, 1937 (2001)
- V.P. Zharov, V.S. Letokhov: *Laser Optoacoustic Spectroscopy*, Springer Ser. Opt. Sci., **37** (Springer, Berlin 1986)
- R. Gerlach, N.H. Amer: *Appl. Phys.* **23**, 319 (1980)
- L.G. Rosengren: *Appl. Opt.* **14**, 1960 (1975)
- C.K.N. Patel, R.J. Kerl: *Appl. Phys. Lett.* **30**, 578 (1977)
- A. Karbach, P. Hess: *J. Chem. Phys.* **84**, 2945 (1986)
- C. Hornberger, M. König, S.B. Rai, W. Demtröder: *Chem. Phys.* **190**, 171 (1995)
- F.G.C. Bijnen, F.J.M. Harren, J. Reuss: *Rev. Sci. Instrum.* **67**, 2914 (1996)
- P. Hess: *Top. Curr. Chem.* **111**, 1 (1983)
- F.J.M. Harren, F.G.C. Bijnen, J. Reuss, L.A.C.J. Voesenek, C.W.P.M. Blom: *Appl. Phys. B* **50**, 137 (1990)
- F.J.M. Harren, R. Berkelmans, K. Kuiper, S. te L. Hekkert, P. Scheepers, R. Dekhuijzen, P. Hollander, D.H. Parker: *Appl. Phys. Lett.* **74**, 1761 (1999)
- K.P. Koch, W. Lahmann: *Appl. Phys. Lett.* **32**, 289 (1978)
- K.H. Fung, H.-B. Lin: *Appl. Opt.* **25**, 749 (1986)
- M. Naegelé, M. W. Sigrist: *Appl. Phys. B* **70**, 895 (2000)
- C.F. Dewey: *Optoacoustic Spectroscopy and Detection*, ed. by Y.H. Pao (Academic Press, New York 1977)
- A. Miklòs, A. Lőrincz: *Appl. Phys. B* **48**, 213 (1989)
- A. Miklòs, P. Hess, A. Mohàcsi, J. Sneider, S. Kamm, S. Schaefer, In: *Photoacoustic and Photothermal Phenomena: 10th International Conference*, ed. by F. Scudieri, M. Bertolotti, AIP Conf. Proc. **463** (AIP, Woodbury 1999) p. 126
- V. Zeninari, V.A. Kapitanov, D. Courtois, Yu.N. Ponomarev: *Infrared Phys. Technol.* **40**, 1 (1999)
- P. Repond, M.W. Sigrist: *Appl. Opt.* **35**, 4065 (1996)
- A.M. Bohren: *Optical Parametric Oscillator Pumped Mid-Infrared Laser Sources for Photoacoustic Trace Gas Spectroscopy*, Ph.D. Thesis No. 12 063, ETH Zürich Switzerland (1997)
- J.B. McManus, P.L. Kebabian, M.S. Zahniser: *Appl. Opt.* **34**, 3336 (1995)
- D. Marinov, M.W. Sigrist: *J. Photopolym. Sci. Technol.* **2**, 774 (2003)
- B. Kolb: *J. Chromatogr. A* **842**, 163 (1999)
- Chemical Properties Handbook*, ed. by C.L. Yaws (McGraw-Hill, New York 1999)
- P.L. Meyer, M.W. Sigrist: *Air Pollution Monitoring With a Mobile CO<sub>2</sub>-Laser Photoacoustic System*, Ph.D. Thesis No. 8651, ETH Zürich Switzerland (1988)
- S. Bernegger, M.W. Sigrist: *Infrared Phys.* **30**, 375 (1990)
- R. Kaestle, M.W. Sigrist: *Appl. Phys. B* **63**, 389 (1996)
- O. Nordhaus, J. Pelzl: *Appl. Phys.* **25**, 221 (1981)
- K. Kupfermüller: *Einführung in die theoretische Elektrotechnik*, 13th edn. (Springer, Berlin, Heidelberg 1990)
- F.C. Karal: *J. Acoust. Soc. Am.* **25**, 327 (1953)
- Gas Encyclopedia*, ed. by L'Air Liquide (Elsevier, Amsterdam 1976)
- V.A. Kapitanov, V. Zeninari, B. Parvitte, D. Courtois, Y.N. Ponomarev: *Spectrochim. Acta A* **58**, 2397 (2002)
- International Critical Tables of Numerical Data, Physics, Chemistry and Technology*, ed. by E.W. Washburn, 1st electronic edition (Knovel, New York 2003)
- P.M. Morse, K.U. Ingard: *Theoretical Acoustics* (Princeton University Press, Princeton 1968)
- International Vocabulary of Basic and General Terms in Metrology*, (ISO, Geneva 1993).
- A.D. Wood, M. Camac, E.T. Gerry: *Appl. Opt.* **10**, 1877 (1971)
- R.A. Rooth, A.J.L. Verhage, L.W. Wouters: *Appl. Opt.* **29**, 3643 (1990)
- M.A. Moeckli, C. Hilbes, M.W. Sigrist: *Appl. Phys. B* **67**, 449 (1998)